Coseismic and postseismic deformation related to the 2007 Chuetsu-oki, Niigata Earthquake

Yusaku Ohta[1], Satoshi Miura[1], Takeshi Iinuma[1], Kenji Tachibana[1], Takeshi Matsushima[2], Hiroaki Takahashi[3], Takeshi Sagiya[4], Takeo Ito[4], Shin'ichi Miyazaki[5], Ryosuke Doke[6], Akira Takeuchi[6], Kayo Miyao[1], Akihiko Hirao[2], Takahiro Maeda[3], Teruhiro Yamaguchi[3], Masamitsu Takada[3], Makiko Iwakuni[5], Tadafumi Ochi[5], Irwan Meilano[4], and Akira Hasegawa[1]

[1]*Research Center for Prediction of Earthquakes and Volcanic Eruptions, Graduate School of Science, Tohoku University, Sendai 980-8578, Japan*
[2]*Institute of Seismology and Volcanology, Faculty of Science, Kyushu University, Shimabara 855-0843, Japan*
[3]*Institute of Seismology and Volcanology, Graduate School of Science, Hokkaido University, Sapporo 060-0810, Japan*
[4]*Graduate School of Environmental Studies, Nagoya University, Nagoya 464-8602, Japan*
[5]*Earthquake Research Institute, University of Tokyo, Tokyo 113-0032, Japan*
[6]*Department of Earth Sciences, Toyama University, Toyama 930-8555, Japan*

(Received December 4, 2007; Revised April 22, 2008; Accepted April 28, 2008; Online published November 18, 2008)

An intermediate-strength earthquake of magnitude M_j 6.8 occurred on July 16, 2007, centered beneath the Japan Sea a few kilometers offshore of Niigata Prefecture in central Japan. We constructed a dense GPS network to investigate postseismic deformation after this event, choosing our GPS sites carefully so as to complement the nationwide GPS GEONET array. Coseismic displacements caused by the mainshock detected at some GEONET sites were used to estimate coseismic fault parameters. The results indicate that the geodetic data can be explained by a combination of two rectangular faults dipping northwest and southeast. Minor but definite postseismic deformation was detected largely in the southern part of the dense network. The time series of site coordinates can be characterized by a logarithmic decay function, and the estimated time constant seems to be almost similar in range to that of the 2004 Mid-Niigata Prefecture Earthquake. We also found a possible site instability at 960566 (Izumo-zaki, GEONET) caused by a small, local landslide associated with the mainshock and therefore concluded that the data obtained at this site should not be used for coseismic or postseismic analysis.
Key words: Crustal deformation, coseismic slip, postseismic deformation, GPS, Niigata-Kobe Tectonic Zone.

1. Introduction

The 2007 Chuetsu-oki Earthquake (M_j 6.8) occurred beneath the Japan Sea a few kilometers offshore of Niigata Prefecture, in central Japan, on 16 July 2007 (Fig. 1). The focal mechanism developed by the Japan Meteorological Agency (JMA) indicates that pure reverse faulting occurred with a NW-SE compression axis. The 2004 Mid-Niigata Prefecture Earthquake on 23 October 2004 was in the inland area of the same prefecture (e.g. Okada *et al*., 2005), and its epicenter was located about 35 km southeast of the 2007 earthquake's epicenter. Sagiya *et al*. (2000) analyzed data from the nationwide GPS network (GEONET, GPS Earth Observation Network System) maintained by the Geographical Survey Institute (GSI) and documented a strain concentration zone extending from Niigata to Kobe, which they called the Niigata-Kobe Tectonic Zone (NKTZ). The epicenters of the 2007 and 2004 events were located within this tectonically active region.

There were not enough GEONET sites near the focal area of the 2007 Niigataken Chuetsu-oki Earthquake to investigate the postseismic deformation related to the earthquake. To obtain more detailed information, immediately after the mainshock, we deployed a dense temporary GPS network composed of 19 stations, which filled the gap in GEONET sites (Fig. 1).

We report there the results of our new GPS observations and discuss the characteristics of coseismic fault models and postseismic crustal movement based on data obtained from GEONET and our temporary sites. The details of the postseismic displacement's spatiotemporal variation are presented in a companion paper by Iinuma *et al*. (2008).

2. GPS Stations and Data Analysis

The new GPS observation sites were constructed immediately after the mainshock by researchers from Tohoku University, Kyushu University, Hokkaido University, and the University of Tokyo. Nagoya University researchers also constructed new GPS sites 1 week after the mainshock. Toyama University researchers had constructed one continuous GPS site (OGNI) after the 2004 Mid-Niigata Prefecture Earthquake, which was still collecting data during the 2007 earthquake. We started observations on July 17 (the day after the mainshock). Figure 1 is a map of the dense GPS network, including our sites and GEONET sites. The GEONET sites are located just around the edge of the mainshock's focal area. For moderately sized inland earthquakes

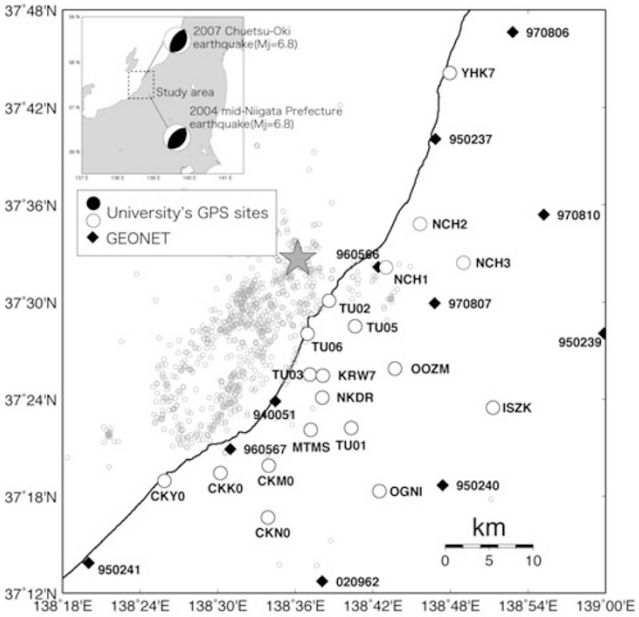

Fig. 1. Location map of GPS sites used in this study and aftershock distribution determined by Kato *et al*. (2008). Open circles denote the temporary GPS sites constructed after the mainshock. The black circle denotes the continuous GPS site operated by Toyama University, which was constructed after the 2004 Mid-Niigata Prefecture Earthquake. Black diamonds indicate GEONET GPS sites. A large star denotes the epicenter of the main shock. Gray circles denote the aftershock distribution.

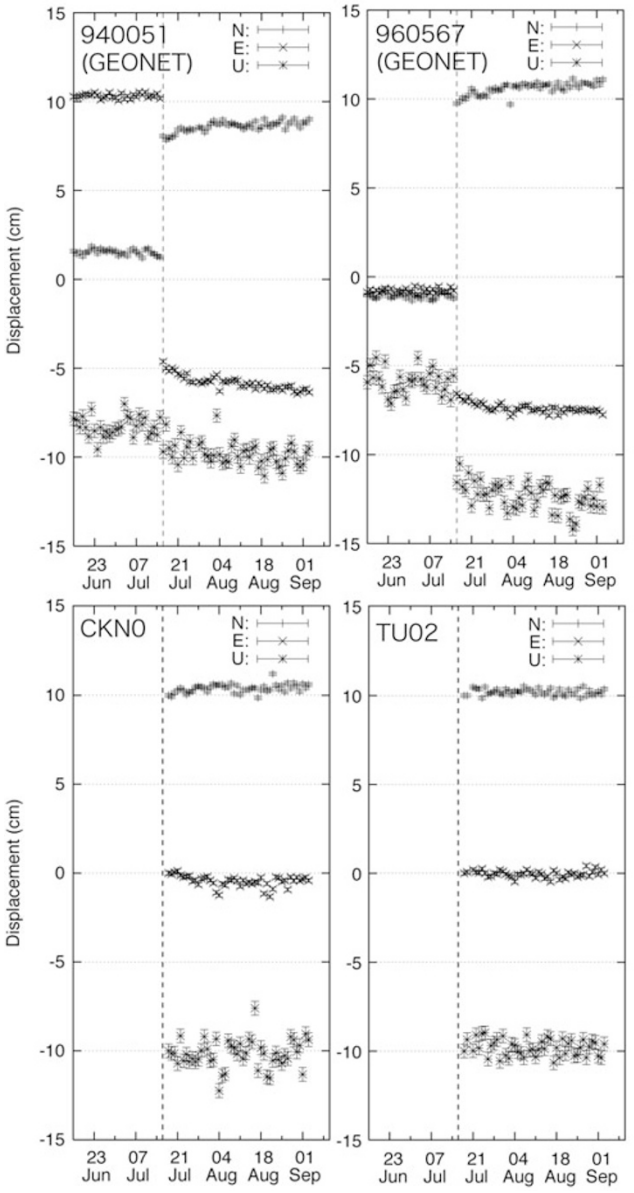

Fig. 2. Time series of daily coordinates at GPS stations with respect to 950231 (Awashima-ura). Upper and lower panels denote GEONET sites and temporary GPS sites deployed in this study, respectively.

with magnitudes between 6.5 and 7.0, GEONET's spatial density is insufficient for determining postseismic displacement. Our new GPS sites, therefore, play a critical role in investigating this phenomenon. GPS antennas were fixed on bolts or self-standing pillars on the roofs of concrete buildings at each site. Dual-frequency GPS receivers were deployed, which sampled code and carrier phase data every 30 s and stored the data in their internal memories and/or in external storage devices.

The program GIPSY/OASIS II version 4.0.4 (Lichten and Border, 1987) was adopted for processing GPS data using the PPP (precise point positioning, Zumberge *et al*., 1997) processing strategy. The PPP method uses data such as precise ephemerides, GPS satellite clock errors, earth rotation parameters, and Helmert's transform parameters, which were provided by the Jet Propulsion Laboratory (JPL), to precisely estimate the site coordinates without any reference sites on the ground. We also used 17 GEONET sites in this analysis. The wet zenith tropospheric delays at all GPS sites were estimated at all processing epochs (every 5 min) under the assumption of a random walk stochastic model with a random walk sigma of 1.7×10^{-7} km $s^{-1/2}$. After PPP processing, we fixed the GEONET site 950231 (Awashima-ura) about 120 km NE of the epicenter (not shown in Fig. 1) as the reference site in this study.

3. Results and Discussion

3.1 Fault model for the mainshock

Figure 2 shows examples of the daily site coordinate time series at four selected sites. At the GEONET sites, the coseismic offset from the main shock was clearly detected. We defined the coseismic displacements as the differences in site coordinates averaged over 2 days before and after the mainshock, respectively. A detailed aftershock distribution was obtained by Kato *et al*. (2008) using the double-difference technique (Zhang and Thurber, 2003) to reveal southeast-dipping alignments of seismicity in the southern part of the focal area. In contrast, aftershock alignments in the northern part are not distinct compared to those of the southern part (Fig. 3), and the geometry of the coseismic fault is still under debate. Based on coseismic displacements, we estimated the fault parameters for each model with two faults dipping NW or SE (Model 1: NW and NW; Model 2: NW and SE; Model 3: SE and NW; Model 4: SE and SE). The rectangular fault parameters in an elastic half space (Okada, 1992) were estimated by a grid search beginning with *a priori* information. We constrained the fault plane location (latitude and longitude), length, width, and dip angle for the grid search estimation. The other pa-

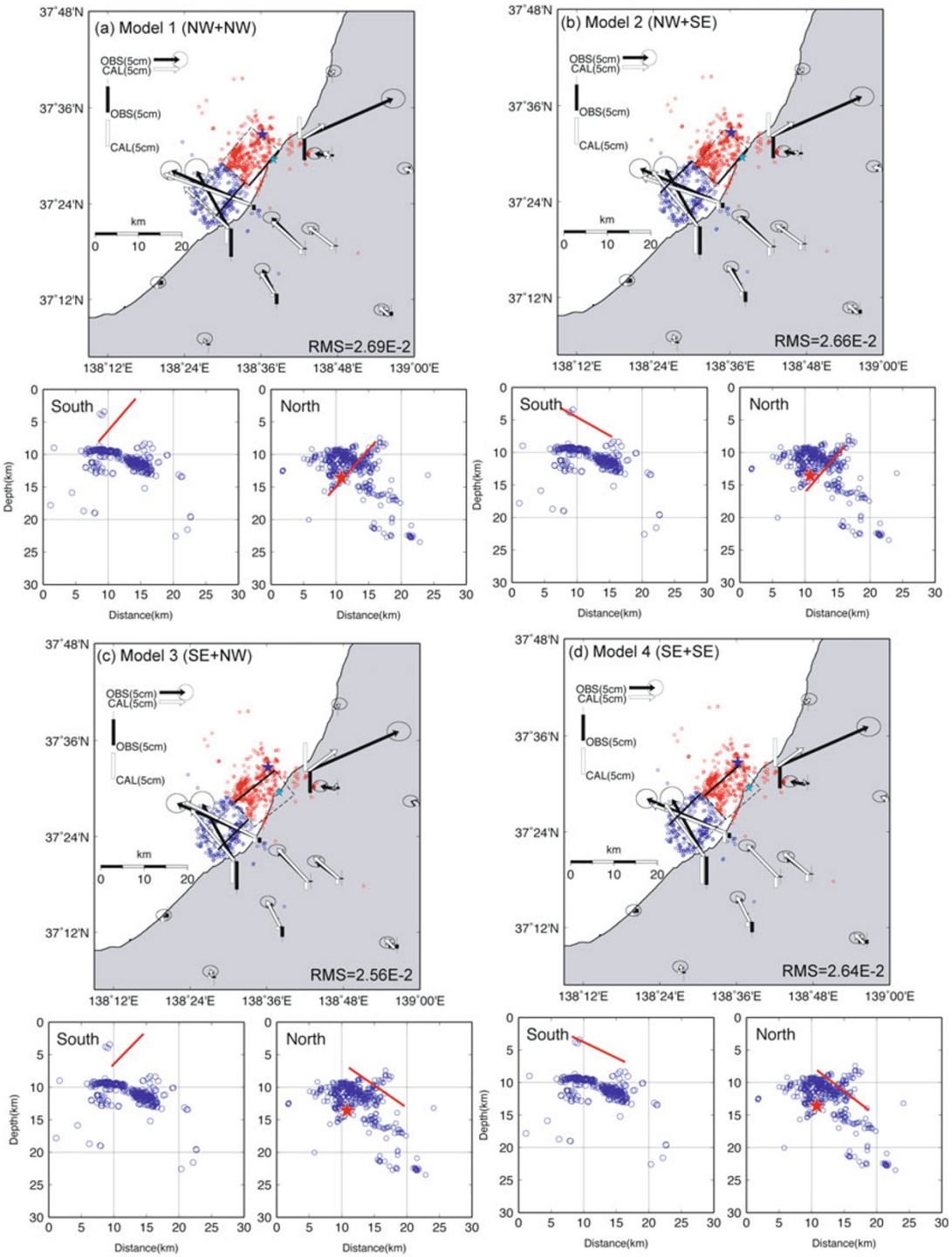

Fig. 3. Comparisons between observed and calculated coseismic displacements, and between the estimated fault geometry and aftershock distribution determined by Kato *et al*. (2008). (a) Combination of NW- and NW-dipping faults for the northern and southern parts of source area, respectively. RMS error is also shown in the figure. (b–d) Same as (a) but for the combination of NW and SE (b), SE and NW (c), and SE and SE (d). Bottom figures of each panel show cross sections of aftershocks (blue) and the fault geometry (red) for the southern (left) and the northern (right) parts of the focal area, respectively. The strike of the cross section is 135° from north to east, which is roughly orthogonal to the strike of each fault. Blue and red stars at the top- and bottom-right of the figures indicate the hypocenter of the main shock.

rameters were estimated without *a priori* information. GSI (2007) reported that the GEONET pillars at 960566 and 960567 (Fig. 1) slightly tilted from the strong ground motion due to the main shock. In Section 3.3, we describe possible site instability of 960566 by co-location observation. By right, we should avoid using 960566 for the coseismic fault model estimation. However, 960566 provides important information for constraining the dimension of the coseismic fault model. Therefore, we assumed a large uncertainty for coseismic displacements (twice the normal value) at these sites. The estimated fault parameters for the four models are listed in Table 1. It is clear that the root-mean-

Table 1. Model parameters of the two rectangular faults with possible combinations of dip angles. Longitude, latitude, and depth denote the location of the upper-left corner of each rectangular fault plane.

Model	Fault plane	Lon. (Deg.)	Lat.(Deg.)	Depth(km)	Length(km)	Width(km)	Str(deg)	Dip(deg)	Rake(deg)	Disp.(m)	Mw	Total Mw	RMS
1	North	138.646	37.511	8.0	10.6	11.8	220.2	45.0	90.1	1.59	6.41	6.63	2.69E−02
NW+NW	South	138.557	37.444	1.4	10.1	9.3	220.4	45.2	89.9	1.85	6.45		
2	North	138.646	37.511	9.0	10.7	9.8	220.1	45.0	90.1	1.75	6.45	6.64	2.66E−02
NW+SE	South	138.419	37.419	3.2	10.4	9.0	45.1	29.4	89.8	2.10	6.43		
3	North	138.517	37.472	7.0	11.8	9.3	51.5	39.1	86.2	1.60	6.35	6.60	2.56E−02
SE+NW	South	138.553	37.436	1.8	10.0	7.0	225.0	45.2	95.7	2.02	6.41		
4	North	138.517	37.476	8.1	10.7	9.6	48.8	40.0	89.9	1.97	6.46	6.61	2.64E−02
SE+SE	South	138.425	37.415	2.9	10.2	9.1	45.0	25.6	89.9	1.49	6.35		

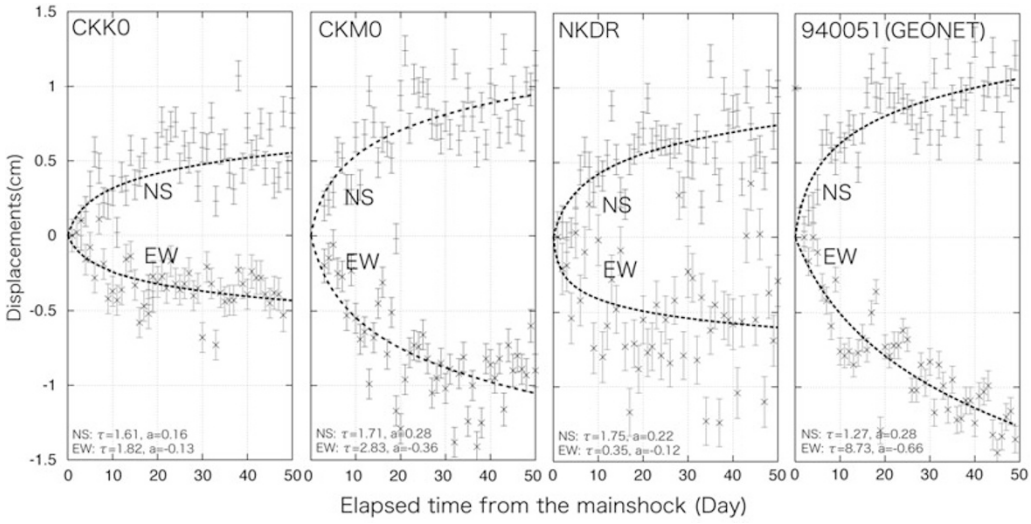

Fig. 4. North-south and east-west displacement components at the GPS sites CKK0, CKM0, NKDR, and 940051 with fitted logarithmic functions. Fitted logarithmic functions' parameters (τ and a) are also shown.

square (RMS) from each of the models is approximately the same, suggesting that we cannot determine the optimal geometry of the two fault plane models only from geodetic data.

However, we can use the aftershock distribution to constrain the geometry of the fault model. If the northern fault dips NW, the hypocenter of the main shock is located on the estimated fault plane (Fig. 3(a) and 3(b)). However, a SE-dipping northern fault segment is not consistent with the location of the main shock hypocenter as the northern fault plane is estimated to be much shallower than the hypocenter (Fig. 3(c) and 3(d)). In contrast, the southern fault plane's aftershock distribution clearly shows the SE-dipping alignment. Furthermore, in both dip angle cases, the estimated fault plane is located 5–7 km shallower than the aftershock distribution (Fig. 3(a–d)). The accuracy of the data on the hypocenter depth of the aftershocks might suffer because the focal area is offshore. The fault geometry accuracy based on the geodetic technique also has some uncertainty for a similar reason. Consequently, on the basis of GPS data and aftershock distribution it is not yet clear precisely which fault plane combination is the more reasonable one.

3.2 Postseismic signals and its characteristics

In the aftermath of the mainshock, we detected minor but clear postseismic displacements at our temporary GPS sites and GEONET sites (Figs. 2 and 4). The maximum postseismic displacement, which is smaller than 3 cm and toward the northwest, was detected at 940051 (GEONET) after 50 days. Understanding the postseismic deformation mechanism is important when investigating an earthquake's cycle. Marone *et al*. (1991) suggested that afterslips obey logarithmic decay functions based on rate- and state-dependent friction laws. A second model for explaining postseismic deformation involves viscoelastic relaxation processes (Scholz, 1990). However, the relaxation times of exponential decay functions predicted by the viscoelastic rebound amount to several months up to years. Sagiya *et al*. (2005) suggested that the decay time of viscoelastic relaxation in the coastal area around the Japan Sea is several years. In this study, we observed a very small postseismic deformation with a short decay time (Fig. 2). Accordingly, we assume that afterslip is the main source of postseismic deformation in this case. To extract the characteristics of the afterslip, we fit the logarithmic function

$$y(t) = a \ln\left(\frac{t}{\tau} + 1\right) \tag{1}$$

to the observed time series, where t is the elapsed time after the mainshock, τ is the decay time constant, and a is the amplitude of the very common logarithmic law for postseismic deformation study (e.g., Takahashi *et al*., 2005; Nakao *et al*., 2006). We estimated a and τ by a non-linear least-squares method.

Figure 4 shows the time series of the northward and eastward displacements at CKK0, CKM0, NKDR, and 940051 with fitted logarithmic curves. The estimated decay time

constants range from 0.35 to 2.83 days, with the exception of that for the eastward component at 940051. This decay time constant range is almost similar to that estimated for the 2004 Mid-Niigata Prefecture Earthquake (M_j 6.8) by Takahashi *et al*. (2005). The 2004 earthquake was an inland shallow earthquake that occurred about 35 km southeast of the 2007 earthquake; if the mechanism and geometry of the afterslip are similar in both earthquakes, the decay time also should be similar. However, the two earthquake fault geometry patterns are significantly different. Thus, it is difficult to provide a detailed discussion on decay time constants at this time.

3.3 Stability of the 960566 (Izumo-zaki) site

As described previously, the GSI reported pillar tilting at sites 960566 and 960567 as a result of strong ground motion due to the mainshock. Site 960566 (Izumo-zaki) is located on the northern edge of the focal area (Figs. 1, 3), and it is an important location for constraining the dimensions of the coseismic and afterslip fault models. Therefore, on 23 July 2007, we constructed a temporary GPS site, NCH1, located 110.7 m away from 960566. If both sites were moved only by postseismic deformation, 960566's time series should show zero displacement relative to NCH1 because of the short distance between them. For confirmation, we investigated the baseline analysis between 960566 and NCH1 using Bernese GPS software version 4.2 (Hugentobler *et al*., 2001) with International GNSS Service (IGS) precise ephemerides and International Earth Rotation Service (IERS) earth rotation parameters. Such a short-baseline (less than 1 km), single-frequency double difference analysis is expected to be quite precise because we can ignore the ionospheric delay between the GPS satellites and the receivers. The tropospheric parameter is also balanced out by double-difference analysis along such a short baseline. Consequently, we estimated the daily position of 960566 relative to NCH1 by single-frequency analysis without estimating the tropospheric parameters.

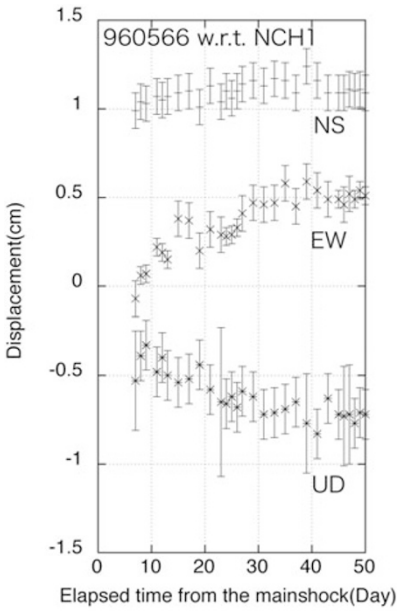

Fig. 5. Time series of 960566 (Izumo-zaki) with respect to the nearby site NCH1 estimated by single-frequency baseline analysis.

Figure 5 shows the displacement time series at 960566 relative to NCH1. Missing daily coordinates in Fig. 5 are caused by the frequent power outages and problems in recording data in the external memory for NCH1. It is clear that 960566 shows afterslip-like eastward and downward movement of several millimeters during the 2–3 weeks after 23 July 2007. In contrast, the northward component demonstrates approximately zero displacement. It is possible that the 960566 site became unstable soon after the mainshock. This site is located on an embankment bordering a school ground. Furthermore, we found a gap of about 1–2 cm between the basement of the 960566 pillar and the surrounding ground on 9 August 2007. The strike of the gap is N315°E, which is roughly orthogonal to the local eastward displacement at the GEONET pillar. We also found some cracks with similar strike directions in the ground around the pillar. Therefore, we conclude that a small-scale landslide took place eastward and downward after the main shock and that site 960566 was affected not only during the coseismic period but also during the postseismic period.

4. Conclusions

We established new temporary GPS sites around the focal region of the 2007 Chuetsu-oki Earthquake (M_j 6.8) immediately after the mainshock. Coseismic displacements caused by the mainshock detected at GEONET sites were used in the coseismic fault model. The results indicate that the geodetic data can be explained by a combination of two rectangular faults dipping toward the northwest and southwest, respectively. Even when compared with aftershock distributions, the geometry of the coseismic fault is still under debate. Postseismic signals were relatively larger at sites in the southern part of the focal area. The estimated coordinate time series were modeled with a logarithmic function and agree with the characteristics of the earthquake's afterslip. We also checked the instability of 960566 by co-location observation. We found possible site instability at 960566 caused by a small, local landslide associated with the strong motion of the mainshock; therefore, the use of this data for coseismic or postseismic analysis should be avoided. In conclusion, such a dense GPS network might provide an important constraint for clarifying events of inland medium-size earthquakes.

Acknowledgments. We gratefully thank the school staff and the local government for permitting us to install the GPS receivers. We are also grateful to the Geodetic Observation Center, GSI, for providing GEONET GPS data. The paper benefited from careful reviews by Dr. Takuya Nishimura (GSI, Japan) and Dr. Laura Wallace (GNS, New Zealand). Focal mechanism data in Fig. 1 were from the JMA database. Dr. Aitaro Kato at Earthquake Research Institute, University of Tokyo, provided the hypocenter data in Figs. 1 and 3. This research was supported by Grants-in-Aid for Scientific Research (representative: Prof. T. Iwasaki), MEXT, of the Japanese Government. Figures were drawn using GMT software (Wessel and Smith, 1991).

References

Geographical Survey Institute (GSI), *Crustal deformation associated with 2007 Niigataken Chuetsu-oki earthquake*, http://www.gsi.go.jp/WNEW/PRESS-RELEASE/2007/0719b.htm, 2007 (in Japanese).

Hugentobler, U., S. Schaer, and P. Fridez, *Bernese GPS Software Version 4.2*, 515 pp., University of Bern, 2001.

Iinuma, T., Y. Ohta, S. Miura, K. Tachibana, T. Matsushima, H. Takahashi, T. Sagiya, T. Ito, S. Miyazaki, R. Doke, A. Takeuchi, K. Miyao, A. Hirao, T. Maeda, T. Yamaguchi, M. Takada, M. Iwakuni, T. Ochi, I. Meilano, and A. Hasegawa, Postseismic slip associated with the 2007 Chuetsu-oki, Niigata, Japan, Earthquake (M 6.8 on 16 July 2007) as inferred from GPS data, *Earth Planets Space*, **60**, this issue, 1087–1091, 2008.

Kato, A., S. Sakai, E. Kurashimo, T. Igarashi, T. Iidaka, N. Hirata, T. Iwasaki, T. Kanazawa, and Group for the aftershock observations of the 2007 Niigataken Chuetsu-oki Earthquake, Imaging heterogeneous velocity structures and complex aftershock distributions in the source region of the 2007 Niigataken Chuetsu-oki Earthquake by a dense seismic observation, *Earth Planets Space*, **60**, this issue, 1111–1116, 2008.

Lichten, S. M. and J. S. Border, Strategies for high precision global positioning system orbit determination, *J. Geophys. Res.*, **92**(B12), 12751–12762, 1987.

Marone, C. J., C. H. Scholz, and R. Bilham, On the mechanics of earthquake afterslip, *J. Geophys. Res.*, **96**, 8441–8452, 1991.

Nakao, S., H. Takahashi, T. Matsushima, Y. Kohno, and M. Ichiyanagi, Postseismic deformation following the 2005 West Off Fukuoka Prefecture Earthquake (M 7.0) derived by GPS observation, *Earth Planets Space*, **58**, 1617–1620, 2006.

Okada, T., N. Umino, T. Matsuzawa, J. Nakajima, N. Uchida, T. Nakayama, S. Hirahara, T. Sato, S. Hori, T. Kono, Y. Yabe, K. Ariyoshi, S. Gamage, J. Shimizu, J. Suganomata, S. Kita, S. Yui, M. Arao, S. Hondo, T. Mizukami, H. Tsushima, T. Yaginuma, A. Hasegawa, Y. Asano, H. Zhang, and C. Thurber, Aftershock distribution and 3D seismic velocity structure in and around the focal area of the 2004 mid Niigata prefecture earthquake obtained by applying double-difference tomography to dense temporary seismic network data, *Earth Planets Space*, **57**, 435–440, 2005.

Okada, Y., Internal deformation due to shear and tensile faults in a halfspace, *Bull. Seismol. Soc. Am.*, **82**, 1018–1040, 1992.

Scholz, C. H., *The Mechanics of Earthquakes and Faulting*, Cambridge University Press, 1990.

Sagiya, T., S. Miyazaki, and T. Tada, Continuous GPS Array and Present-day Crustal Deformation of Japan, *PAGEOPH*, **157**, 2303–2322, 2000.

Sagiya, T., M. Ohzono, S. Nisiwaki, Y. Ohta, T. Yamamuro, F. Kimata, and M. Sasaki, Postseismic Deformation Following the 2004 Mid-Niigata Prefecture Earthquake around the Southern Part of the Source Region, *Zisin 2*, **58**, 359–369, 2005 (in Japanese with English abstract).

Takahashi, H., T. Matsushima, T. Kato, A. Takeuchi, T. Tamaguchi, Y. Kohno, T. Katagi, J. Fukuda, K. Hatamoto, R. Doke, Y. Matsu'ura, and M. Kasahara, A dense GPS observation immediately after the 2004 mid-Niigata prefecture earthquake, *Earth Planets Space*, **57**, 661–665, 2005.

Wessel, P. and W. H. F. Smith, Free software helps map and display data, *EOS Trans. AGU*, **72**, 441, 1991.

Zhang, H. and C. H. Thurber, Double-difference tomography: The method and its application to the Hayward fault, California, *Bull. Seismol. Soc. Am.*, **93**, 1875–1889, 2003.

Zumberge, J. F., M. B. Heflin, D. C. Jefferson, M. M. Watkins, and F. H. Webb, Precise point positioning for the efficient and robust analysis of GPS data from large networks, *J. Geophys. Res.*, **102**(B3), 5005–5017, 1997.

Y. Ohta (e-mail: ohta@aob.geophys.tohoku.ac.jp), S. Miura, T. Iinuma, K. Tachibana, T. Matsushima, H. Takahashi, T. Sagiya, T. Ito, S. Miyazaki, R. Doke, A. Takeuchi, K. Miyao, A. Hirao, T. Maeda, T. Yamaguchi, M. Takada, M. Iwakuni, T. Ochi, I. Meilano, and A. Hasegawa